AGU PUBLICATIONS

JGR

Journal of Geophysical Research: Space Physics

RESEARCH ARTICLE

10.1002/2014JA020300

Key Points:
- Good correlation of westward drift rate VS $F_{10.7}$ is found with continuous data
- Besides the known northward drift, the southward drift of SAA is also found
- Possible cause of the two new findings is discussed with simulation results

Correspondence to:
X. Zhang,
zhangxg@nssc.ac.cn

Citation:
Qin, M., X. Zhang, B. Ni, H. Song, H. Zou, and Y. Sun (2014), Solar cycle variations of trapped proton flux in the inner radiation belt, *J. Geophys. Res. Space Physics*, *119*, 9658–9669, doi:10.1002/2014JA020300.

Received 21 JUN 2014
Accepted 5 NOV 2014
Accepted article online 11 NOV 2014
Published online 4 DEC 2014

Solar cycle variations of trapped proton flux in the inner radiation belt

Murong Qin[1,2], Xianguo Zhang[2], Binbin Ni[3], Hongqiang Song[1], Hong Zou[4], and Yueqiang Sun[2]

[1]Shandong Provincial Key Laboratory of Optical Astronomy and Solar-Terrestrial Environment, Institute of Space Sciences, Shandong University, Weihai, China, [2]Laboratory of Space Environment Exploration, Center for Space Science and Applied Research, Chinese Academy of Sciences, Beijing, China, [3]Department of Space Physics, School of Electronic Information, Wuhan University, Wuhan, China, [4]Institute of Space Physics and Applied Technology, Peking University, Beijing, China

Abstract Trapped proton population in the inner radiation belt is highly dense, posing a potential danger to astronauts and man-made space assets traversing through this region. While being significantly stable within timescales up to hundreds of days, inner zone proton fluxes can exhibit considerable solar cycle variations, which has not been investigated comprehensively yet. To analyze the long-term variation of the South Atlantic Anomaly (SAA), we adopt the proton flux data measured by NOAA 15 from 1999 through 2009 and perform statistical analyses on the basis of reasonable Gaussian fits. We report that the variation of the peak proton flux in the SAA is anticorrelated with that of $F_{10.7}$ during a solar cycle. There also exists a phase lag of 685 days between the solar $F_{10.7}$ flux and the proton flux. Similar features are seen for changes of the SAA distribution area, which in addition shows a rapid decrease during the solar maximum and a slow increase during the solar minimum. We also find that the region where the proton flux peaks drifts westward year by year with larger drift rates during the solar minimum. The peak region shifts southward during the solar maximum but in the opposite direction during the solar minimum with higher shift speed. Enhancements in solar wind dynamic pressure can favor the north-south drift of the SAA.

1. Introduction

The trapped radiation environment, consisting of large amounts of energetic charged particles, can be potentially harmful to human beings and space vehicles immerged in it. Since the geomagnetic field is not a perfect dipole, the inner radiation belt gets closer to the Earth over the South Atlantic Ocean, which is called the South Atlantic Anomaly (SAA) [*Kurnosova et al.*, 1962]. Exposed to stronger radiation, low-Earth orbiting (LEO) spacecrafts suffer much higher risks of being damaged in this region. In order to understand the complex mechanisms of energetic particle source and loss for monitoring the dynamic radiation environment and mitigating the underlying hazards, an extensive investigation of the statistical variation of inner zone energetic proton flux within different time scales in the SAA is essential and is the focus of the present study.

A typical temporal variation in this region is the solar cycle variation [*Nakano and Heckman*, 1968; *Dragt*, 1971]. The proton flux variation was first substantiated to be anticorrelated with solar cycle changes in density of the upper atmosphere on the basis of experimental data [*Nakano and Heckman*, 1968]. Using data from the TIROS/NOAA spacecraft, *Huston et al.* [1996, 1998] found a definite phase lag when examining the anticorrelation relationship between the $F_{10.7}$ flux and the proton flux. It was further shown that the phase lag is correlated with L and B [*Huston et al.*, 1998; *Huston and Pfitzer*, 1998; *Kuznetsov et al.*, 2010] (B is the magnetic field magnitude at the point of measurement and L is the McIlwain parameter for a trapped particle mirroring at this point [*McIlwain*, 1966]).

Other features of the SAA solar cycle variation were also examined, such as the temporal evolution of the center and shape of the SAA, by using a fitted function. The traditional mode is the Gaussian fit [*Konradi et al.*, 1994; *Badhwar et al.*, 1994; *Bühler et al.*, 1996]. By analyzing the data measured in two individual time periods with a gap of about 11 years, an average westward drift rate ranging from 0.26°/yr to 0.34°/yr was found. Recently, based on available long-term, continuous data, *Fürst et al.* [2009] and *Hell* [2010] put forward the Weibull fit and the Gumbel fit, respectively, to study the behaviors of the SAA. They acquired useful temporal information of the SAA strength and its peak longitude position. By analyzing the noise induced by nighttime particles, *Casadio and Arino* [2011] implemented the fitting using a two-dimensional, elliptical Gaussian function to investigate the solar cycle variation of the strength, position, and extension of the SAA.

The westward drift rate of the SAA obtained with different methods or different types of particles differs substantially. It can vary between 0.18 ~ 0.66°/year based on previous studies [*Badhwar et al.*, 1994; *Konradi et al.*, 1994; *Bühler et al.*, 1996; *Heynderickx*, 1996; *Pu et al.*, 2005; *Xie et al.*, 2005; *Ginet et al.*, 2007; *Fürst et al.*, 2009]. In fact, the westward drift rate is not constant and has been proposed to exhibit a solar cycle variation [*Grigoryan et al.*, 2008]. Another explanation for variation in the westward drift rate is geomagnetic jerk, which is a jump in the second derivative of the magnetic field strength and occurs due to a jump in the acceleration in the fluid motion at the core-mantle-boundary [*Olsen and Mandea*, 2007]. *Fürst et al.* [2009] thought that the two breaks in the drift rate in 1998 and 2003 could be possibly connected to the geomagnetic jerks that occurred approximately at the same time. However, it cannot explain the substantial difference in the impact of different geomagnetic jerks on the SAA evolution [*Hell*, 2010]. Whether changes of the SAA should be attributed to geomagnetic jerks or the solar cycle variation of the atmosphere remains an open question.

A northward drift of the SAA was also observationally confirmed. The shifts of SAA over the 21.2 year time give an average drift rate of 0.08°/yr in latitude [*Badhwar*, 1997]. While the solar cycle variation of the latitudinal center of the SAA was studied analyzing the nighttime particle induced noises [*Casadio and Arino*, 2011], the latitudinal drift of the SAA during different phases of a continuous solar cycle needs a further comprehensive investigation based on direct observations.

(B, L) [*McIlwain*, 1966] coordinate system can be used to describe the radiation belt features, but the position and shape of the SAA cannot be reconstructed using this method. In order to avoid the influence of the data gap and the statistical fluctuation associated with direct observations, as an alternative, methods by curve fitting can be applied to investigate the strength, location, and area of the SAA, i.e., the peak proton flux, the location of the local particle flux maximum, and the area where protons distribute over the region of the SAA. In this study we adopt the Gaussian fitting method to investigate the SAA characteristics.

The high-energy proton observations of 80–215 MeV proton channels measured by the detectors onboard NOAA 6, NOAA 10, NOAA 12, and of > 16 MeV, > 35 MeV, > 70 MeV, and > 140 MeV proton channels measured by NOAA 15 are adopted to establish the analysis database. In the following sections, we will report direct evidence of the behaviors of proton flux in the SAA by performing a comprehensive survey of its temporal evolution and spatial distribution. The differences in variation rate between the solar maximum and the solar minimum will be emphasized, and the specific delay time associated with the hysteresis effect will be evaluated. In addition, factors that can contribute to the solar cycle variation of the SAA drift will be investigated along with discussions of possible mechanisms.

2. Data

2.1. Instrumentation and Data Archive

TIROS /NOAA are a series of low-altitude, polar-orbiting meteorological satellites launched by the U.S. National Oceanic and Atmospheric Administration (NOAA) since 1978. Launched into about 800 km low Earth orbit with an inclination of 98° and an orbital period of about 101 min, these satellites can be divided into two sets according to their Space Environment Monitors (SEM), which can in situ detect the proton and electron fluxes along the satellite orbits. The first set begins from TIROS to the NOAA 14 satellite, onboard which are SEM 1 instruments. The second set begins from the NOAA 15 satellite with an upgraded version of the Space Environment Monitor (SEM 2). The SEM consists of the following equipments: Medium Energy Proton and Electron Detector (MEPED), Total Energy Detector (TED), and High-Energy Proton and Alpha Detector (HEPAD) [*Evans and Greer*, 2000]. The MEPED is a collection of directional detectors and omnidirectional sensors. Each omnidirectional sensor consists of a dome of moderating material which absorbs energy from the particle and so sets the detection energy threshold. The primary data used in the present study comes from the particle measurements from NOAA 6 (1 January 1980 to 18 August 1986), NOAA 10 (11 October 1986 to 27 January 1991), NOAA 12(1 January 1992 to 1 March 2002), and NOAA 15 (1 January 1999 to 12 December 2009).

In order to concentrate on studying the high-energy proton flux in the inner radiation belt, the data from omnidirectional proton detectors of MEPED are selected for the following analyses. For SEM 1, protons with energy of 80–215 MeV are used to study the solar cycle variation. For SEM 2, data over the period of 1999–2009 on board NOAA 15, which covers the whole 23rd solar cycle, are used to examine the quantitative correlation between the variations of the SAA and the $F_{10.7}$. Downloaded from

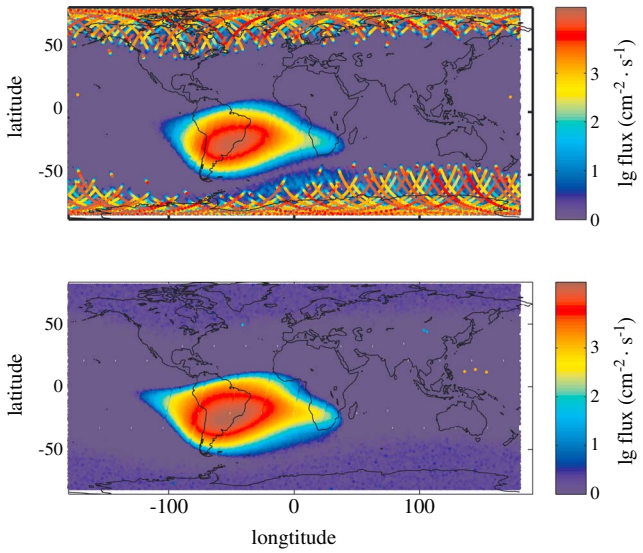

Figure 1. Two examples showing (top) the distribution of SAA proton fluxes during the solar proton events in November 2001 and (bottom) the distribution of SAA proton fluxes during a geomagnetically quiet period in November 2009.

http://www.swpc.noaa.gov/ftpmenu/indices/old_indices.html, the 10.7 cm solar flux ($F_{10.7}$) data are used as indicator of solar activity.

2.2. Preprocessing of Data

Proton population in Earth's radiation belts is highly dynamic, which is influenced by various complicated factors, such as (1) the solar proton events in which the proton flux will increase suddenly in a short period, including the LEO altitude within the middle- and high-latitude regions; (2) the collision effects between the upper atmosphere of the Earth and the protons, which can decrease the flux; (3) the albedo neutron decay which can increase the Cosmic Ray Albedo Neutron Decay (CRAND) proton population at middle and high latitudes; (4) the long-term variation of the geomagnetic field, which can contribute to the gradual change of the proton flux. Solar proton events occur occasionally [*Shea and Smart*, 1990] with increased occurrence probability with solar activity. The enhancement of solar activity can also result in density increase in the upper atmosphere, thus leading to decrease of the proton flux. In addition, due to the close connection of the external component of the geomagnetic field with the solar terrestrial current system, it is reasonable to anticipate that the variation of proton flux associated with the secular change of the geomagnetic field tend to bear certain solar cycle characteristics. Under all these considerations, here we focus on the solar cycle variation of the proton flux, which can be correlated with the latter two factors. Therefore, a preprocessing procedure to subtract the effect of the first factor needs to be performed. Since the energetic protons with energies > 10 MeV do not remain trapped at high L shells and hence do not exist during geomagnetically quiet times above certain L values due to their large gyroradii, these protons are considered to only appear in the inner radiation belt at low L values during most time periods and only exist at high L briefly during the solar proton events, as shown in Figure 1.

Therefore, the data during those days when the flux of > 16 MeV protons in the high-latitude region was more than 20 cm^{-2} · s^{-1} is excluded from the database before our comprehensive analysis.

3. Analysis Results

3.1. SAA Spatial Distribution

The SAA region for protons > 16 MeV covers an area with a latitudinal range from −60° to 10° and a longitudinal range from −110° to 20°. From its center to the boundary, the proton flux decreases exponentially along with latitude and longitude, respectively; thus, it can be a reasonable treatment to fit the proton flux in the SAA using a Gaussian function. The Gaussian distribution is assumed to follow the form,

$$y = a \cdot e^{\frac{-(x-b)^2}{c^2}} \tag{1}$$

When applying to the distribution of the SAA proton flux, a is a quantity representative of the maximum of the proton flux, b is the position where the proton flux peaks, c is the half width of the SAA over latitude or longitude where the $1/e$ peak proton flux appears, y is the proton flux measured by MEPED, and x is the latitude or longitude where the proton flux y is sampled.

To gauge the quality of Gaussian fit, an example for proton > 70 MeV over the period from 20 March 2003 to 20 June 2003 and the corresponding analysis is shown in Figure 2. Figures 2a1 and 2a2 show the Gaussian fit result over latitude for the data between longitudes of −53° to −47°, which we selected as

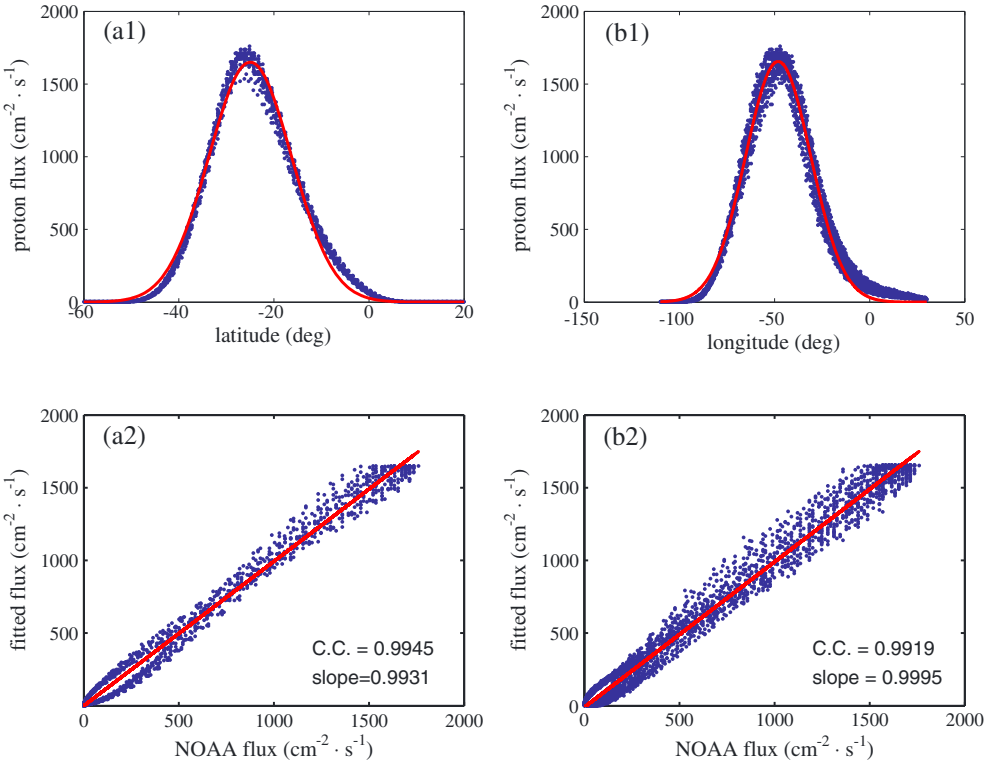

Figure 2. Gaussian fitting results as a function of experimental NOAA flux for protons > 16 MeV over the period from 20 March 2003 to 20 June 2003: (a1, a2) for a longitudinal range of −53° to −47°, and (b1, b2) for a latitudinal range of −28° to −22°.

the core peak longitude location of the proton flux in the SAA for the 23rd solar cycle. Figures 2b1 and 2b2 show the Gaussian fit over longitude for the data between latitudes of −28° to −22°, which we selected as the core peak latitude location of the proton flux in the SAA for the 23rd solar cycle. Figures 2a1 and 2b1 show the fitting examples. The blue dots are the experimental data and the superposed red lines are the Gaussian fit results. Figures 2a2 and 2b2 show the Gaussian fit result as a function of experimental NOAA flux and the corresponding correlation coefficient between them. The blue dots show the correlation between the experimental proton flux and the Gaussian fit results. Superposed to the data is a linear fit to the data (red solid line). It can be seen that (1) the correlation coefficients of the Gaussian fits are close to 1, which demonstrates that the 1-D Gaussian function is a suitable form to describe the longitudinal or latitudinal distribution of the SAA; (2) the slopes of the linear fits are also close to 1, which demonstrates that the fit result is quite close to the measured value. Such an example clearly indicates that using a Gaussian function can favorably reconstruct the proton flux distribution in the SAA. As a consequence, it justifies that modelled parameters of Gaussian fitting can act as reasonable proxies to investigate the particle flux distribution in the SAA.

In the process to determine the peak location, the proton flux is fitted with respect to the latitude in a 6° longitudinal boxcar near the west boundary of the SAA. By moving the boxcar 1° eastward every time, a series of peak proton flux and the corresponding longitudinal boxcar of a random month are obtained. The longitudinal boxcar with the maximum peak proton flux is selected as the longitudinal center separation. Similar method is also applied to obtain the latitudinal center separation. The longitudinal center separations for NOAA 6, NOAA 10, NOAA 12, NOAA 15 (> 70 MeV) are [−48°, −42°], [−50°, −44°], [−52°, −46°, and [−53°, −47°], respectively, while the latitudinal center are all within the range of [−28°, −22°]. As a matter of fact, both the longitudinal and latitudinal centers of the SAA move within the separations mentioned above during the long period investigated in this study.

The processed data is divided into a series of bins with a discrete, continuous time window of 3 months in order to improve the spatial resolution in every bin and minimize the potential errors associated with Gaussian fitting. Fits to the flux latitude distribution and to the flux longitude distribution are performed

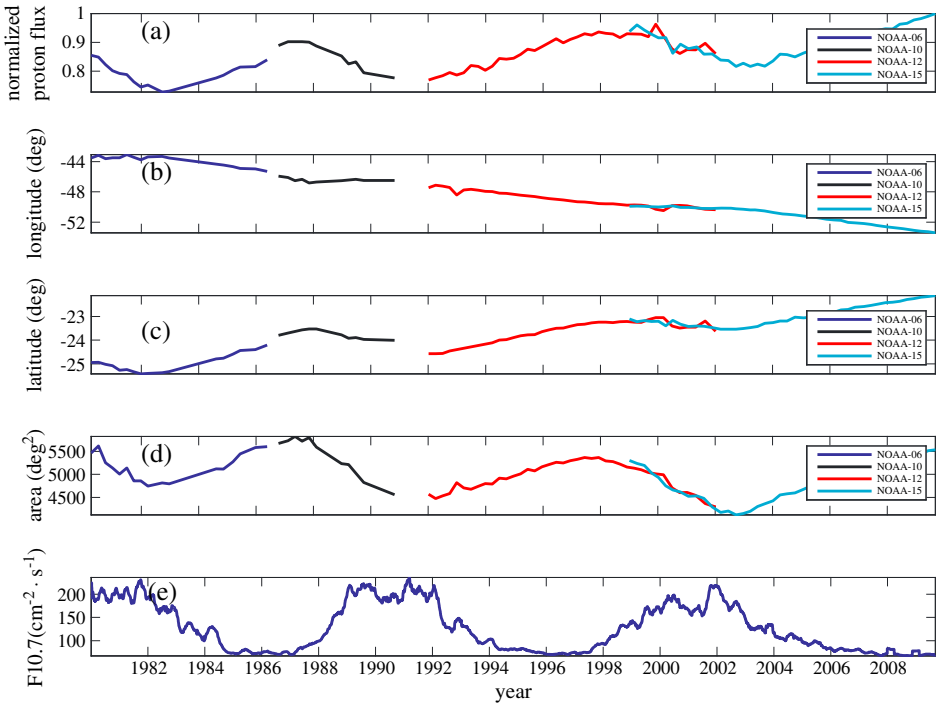

Figure 3. Temporal evolution of (a) the normalized peak proton flux, (b) longitudinal center, (c) latitudinal center and (d) the area of the SAA, and (e) $F_{10.7}$. The blue, black, and red solid lines correspond to the data from NOAA 6, NOAA 10, NOAA 12, and NOAA 15 satellite, respectively.

constantly within the separations of longitudinal and latitudinal center, respectively. To deal with this situation, a series of proton peak fluxes a and corresponding longitudinal or latitudinal position b at different time intervals are calculated.

Furthermore, the boundary position of the SAA can also be calculated by setting a specific proton flux, for example, a value of 100 cm^{-2} · s^{-1} adopted here. Equation (1) can be converted into

$$x = \pm\sqrt{-c^2 \ln \frac{y}{a}} + b \tag{2}$$

From equation (2), we can obtain a series of x values, which represent the latitudinal or longitudinal boundary position of the SAA, given the fitted parameters a, b, and c. Subsequently, the SAA area can be evaluated as a multiple of north-south boundary distance and east-west boundary distance.

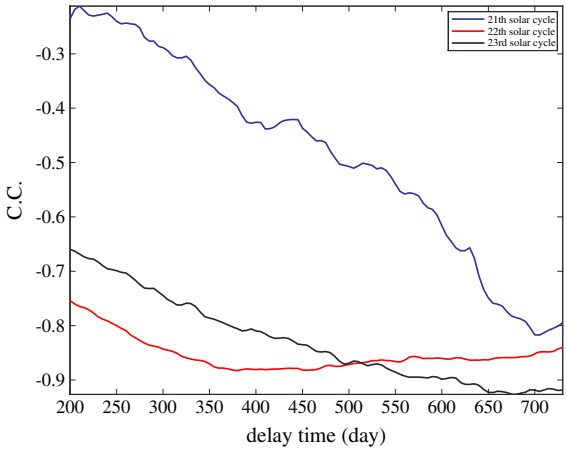

Figure 4. Anticorrelation coefficient between the peak SAA proton flux and the $F_{10.7}$ flux as a function of time lag. Blue line for the 21st solar cycle (1 January 1980 to 21 December 1986), red line for the 22nd solar cycle (8 February 1987 to 1 June 1999) and black line for 23rd solar cycle (1 January 1999 to 30 December 2009).

3.2. SAA Temporal Evolution

The solar activity indicator $F_{10.7}$ is downloaded from the Space Weather Prediction Center (SWPC). The original data are discontinuous due to the different instruments and energies. In order to get a consecutive evolution of the SAA, the data of different satellites are cross calibrated. Figure 3 shows the temporal evolution of the strength, the longitude center, the latitudinal center and the area of

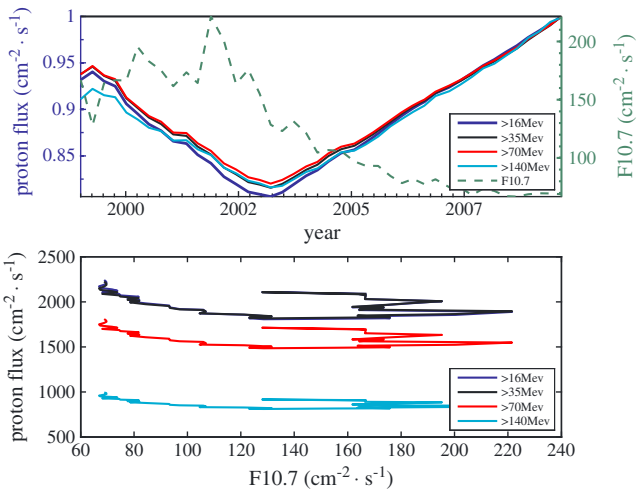

Figure 5. (top) Temporal variations of the smoothed $F_{10.7}$ flux normalized by the maximum $F_{10.7}$ value in this interval (dashed curve) and the normalized peak proton fluxes for the indicated four proton energy channels (color-coded solid curves). (bottom) Proton flux versus $F_{10.7}$ for the considered four proton energy channels.

the SAA, and the corresponding $F_{10.7}$. The blue, black, red, and cyan solid lines correspond to the data from NOAA 6, NOAA 10, NOAA 12, and NOAA 15 (> 70 MeV), respectively.

It is shown that all the above four variables of the SAA show solar cycle characteristics: (1) The local maximum SAA proton flux increases during the solar minimum and decreases during the solar maximum; (2) The center of the SAA drifts westward faster in solar minimum than in solar maximum; (3) The center of the SAA drifts southward during the solar maximum and northward during the solar minimum; (4) The area of the SAA decreases during the solar maximum and increases during the solar minimum.

A phase lag also occurs between $F_{10.7}$ and the maximum SAA proton flux. We fit $F_{10.7}$ and the proton flux using different delay times. As shown in Figure 4, we capture the highest correlation coefficient with a time delay of 705 days of the 21st solar cycle (1 January 1980 to 21 December 1986), 380 days of the 22nd solar cycle (8 February 1987 to 1 June 1999) and 685 days of the 23rd solar cycle (1 January 1999 to 30 December 2009).

3.3. Correlation Between Variation of the SAA and the $F_{10.7}$

In order to obtain a continuous, quantitative correlation between the $F_{10.7}$ and the SAA, data from NOAA 15, which is the only satellite that covers a whole solar cycle, are used here for in-depth investigation.

3.3.1. Peak Proton Flux and the Phase Lag

Figure 5 (top) shows the solar cycle variation of the normalized, smoothed $F_{10.7}$ and the normalized peak SAA proton flux for the period of 1999–2009 of our interest. There are several major features that can be addressed:

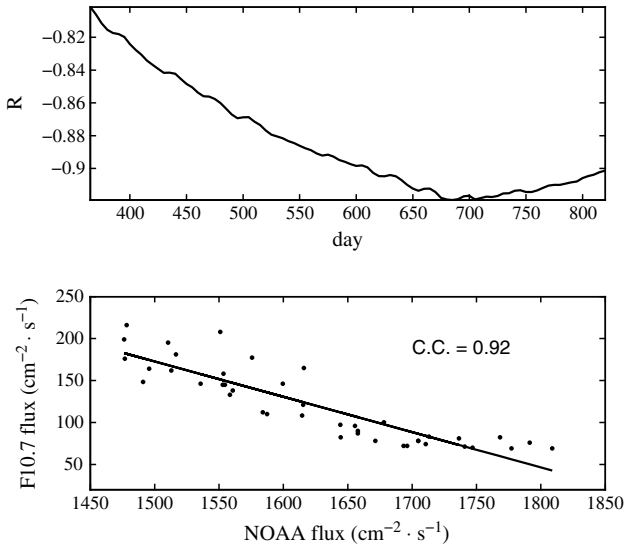

Figure 6. (top) Anticorrelation coefficient between the peak SAA proton flux and the $F_{10.7}$ flux as a function of time lag. (bottom) Functional relationship between the $F_{10.7}$ cm flux and the peak SAA proton flux with an allowance of 685 day delay.

1. An anticorrelation trend occurs between the two quantities. The local maximum SAA proton flux increases during the solar minimum and decreases during the solar maximum;
2. The local maximum of the SAA proton flux is larger during the solar cycle declining phase than during the climbing phase;
3. A phase lag also occurs between $F_{10.7}$ and the maximum SAA proton flux. Figure 5 (bottom) shows the proton flux plotted as a function of $F_{10.7}$ for different energy channels. The hysteresis effect, that is, the proton flux varies at a fixed value of $F_{10.7}$ between the growing and falling phase of the solar cycle, is apparently registered;

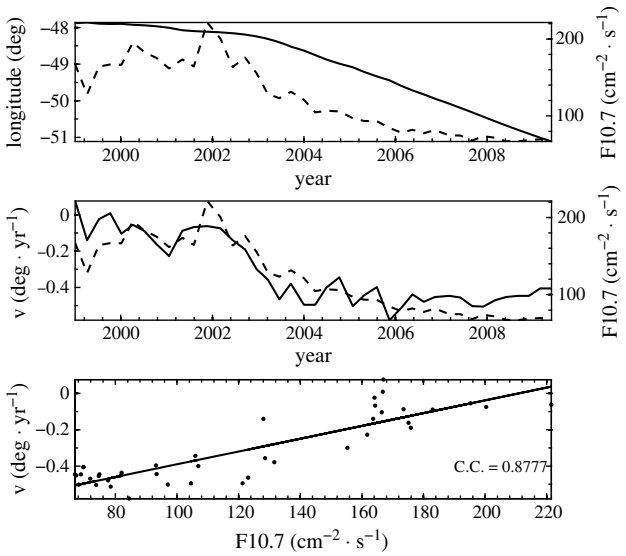

Figure 7. Secular variation of (top) the longitudinal position of the peak SAA proton flux and (middle) the eastward drift velocity of the SAA. (bottom) The westward drift rate and its linear fit as a function of the $F_{10.7}$ flux. The dashed curves show the averaged $F_{10.7}$ cm flux from 1999 through 2009.

4. The variation trends are approximately the same with respect to the four energy channels in our research. Hence, the subsequent analyses only concentrate on one energy channel, i.e., > 70 MeV, representative of other MEPED proton energy channels. We fit $F_{10.7}$ and the proton flux using different delay times. As shown in Figure 6 (top), we capture a highest correlation coefficient 0.92 with a time delay of 685 days. Correspondingly, the lower panel of Figure 6 depicts the variation of peak SAA proton flux with the $F_{10.7}$ flux after applying a time delay of 685 days, which clearly demonstrates an anticorrelated relationship between them.

3.3.2. Movement of the SAA

The solar cycle variation of the smoothed 3-monthly longitudinal position of the proton flux peak is shown in Figure 7 (top). It illustrates that the longitudinal center of the SAA drifts westward about 3.3° in the considered 11 years. The average drift rate is 0.3° per year, in good agreement with previous studies [*Badhwar et al.*, 1994; *Konradi et al.*, 1994; *Bühler et al.*, 1996]. Figure 7 (middle) shows more details of the longitudinal drift rate of the SAA proton flux peak. Apparently, the drift rate changes year by year. During the solar maximum (1999–2003), the average drift rate is 0.12° per year. In contrast, the average drift speed is 0.45° per year during the solar minimum, a factor of ~ 3 faster than that during the solar maximum. In addition, the longitudinal drift rate is highly correlated with the $F_{10.7}$, as indicated in Figure 7 (bottom) that plots the drift rate along with $F_{10.7}$. The correlation coefficient is 0.8777.

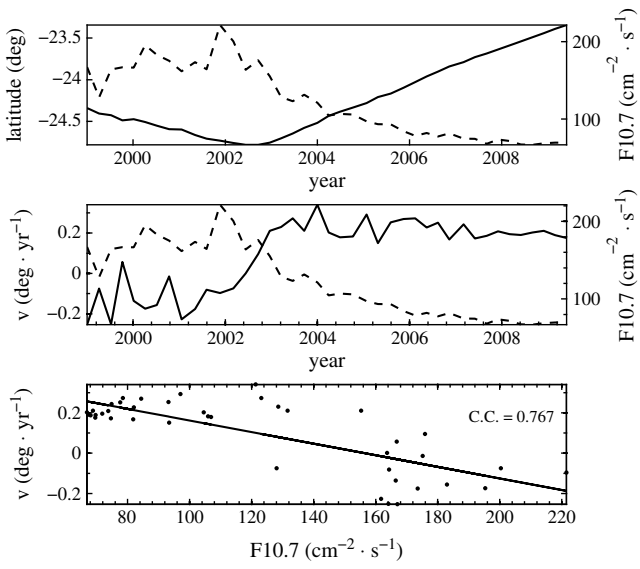

Figure 8. Secular variation of (top) the latitudinal position of the peak SAA proton flux and (middle) the northward drift velocity of the SAA. (bottom) The northward drift rate and its linear fit as a function of the $F_{10.7}$ flux. The dashed curves show the averaged $F_{10.7}$ cm flux from 1999 through 2009.

The solar cycle variation of the smoothed 3-monthly latitudinal position of the proton flux peak is shown in Figure 8 (top). It shows that the center of the SAA drifts southward during the solar maximum and northward during the solar minimum. It drifts northward about 1° in 11 years. The average drift speed is about 0.09° per year. The drift speed of the SAA latitudinal center is slower during the solar maximum compared to that during the solar minimum. Specifically, as shown in Figure 8 (middle), the SAA latitudinal drift is southward with a rate of 0.085° per year during the solar maximum, while it is northward with a speed of 0.219° per year during the solar minimum. Figure 8 (bottom) further illustrates that the latitudinal drift rate of the SAA is approximately correlated with the $F_{10.7}$ flux. The correlation coefficient

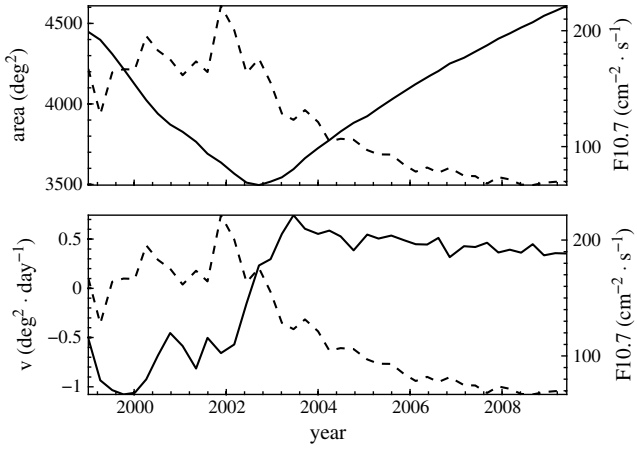

Figure 9. (top) Solar cycle variation and (bottom) variation rate of the SAA area. The dashed curves show the averaged $F_{10.7}$ cm flux from 1999 through 2009.

between them is 0.767, lower than that between the longitudinal drift rate and the $F_{10.7}$ flux.

3.3.3. Extension of the SAA

We also study the temporal evolution of the area of the SAA, the results of which are shown in Figure 9. It is demonstrated that the area of the SAA is also inversely correlated with the $F_{10.7}$ flux (Figure 9, top) and that it decreases rapidly during the solar maximum and increases slowly during the solar minimum (Figure 9, bottom). The rates of the decrease and increase are 0.59 deg^2 per day and 0.47 deg^2 per day, respectively. The area of SAA is larger during the solar cycle declining phase than the climbing phase, indicating that the SAA can expand with the entire solar cycle.

3.3.4. The B_{min} Position of the SAA

The minimum magnetic field (B_{min}) position of the SAA is calculated using the International Geomagnetic Reference Field (IGRF) model, the results of which are shown in Figure 10. Figure 10 (top) shows the secular variation of the longitudinal B_{min} corresponding to an altitude of 808 km and a latitude of −23°, and Figure 10 (bottom) shows the secular variation of the latitudinal B_{min} corresponding to an altitude of 808 km and a longitude of −52°. It shows that the internal magnetic field drifts westward and northward slowly without showing any solar cycle characteristics.

We further adopt the *Tsyganenko* [1995] geomagnetic field model (T96) to calculate the latitudinal position of the geomagnetic field minimum. The results of which are shown in Figure 11. Three indices are considered: the solar wind dynamic pressure P_{dyn}, B_z component of the interplanetary magnetic field B_{zIMF}, and *Dst*. In Figure 11a, we assume that the solar wind dynamic pressure follows the equation $y = 2 + 8 \cdot sin\frac{(x-1998)\pi}{16}$ with x as the number of the year. The temporal variation of P_{dyn} is shown as the red dashed line. We further assume that other two considered indices B_{zIMF} and *Dst* are time constant. For this case, it is clear that the latitudinal position of the geomagnetic field minimum (red solid line) drifts southward quickly after the solar wind dynamic pressure increases to a high value. In contrast, Figure 11b and 11c show that the other two parameters, B_{zIMF} and *Dst*, have little effect on the variation of the B_{min} position of the SAA within a solar cycle.

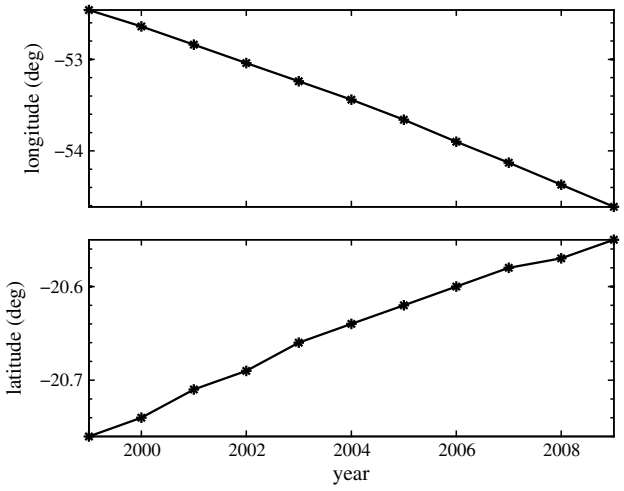

Figure 10. Secular variation of (top) the longitudinal center and (bottom) the latitudinal center of the SAA with the adoption of the IGRF magnetic field.

A similar analysis with the adoption of T96 model is also applied to examine the temporal evolution of the longitudinal position of the SAA B_{min}, as shown in Figure 12. The results show no clear dependence of the longitudinal position of the SAA B_{min} on the considered parameters.

4. Discussions

In the present study we have adopted the method of Gaussian fitting to analyze the solar cycle variation of the proton flux in the SAA over three cycles (1980–2009). Continuous, quantitative analysis has been conducted in terms of

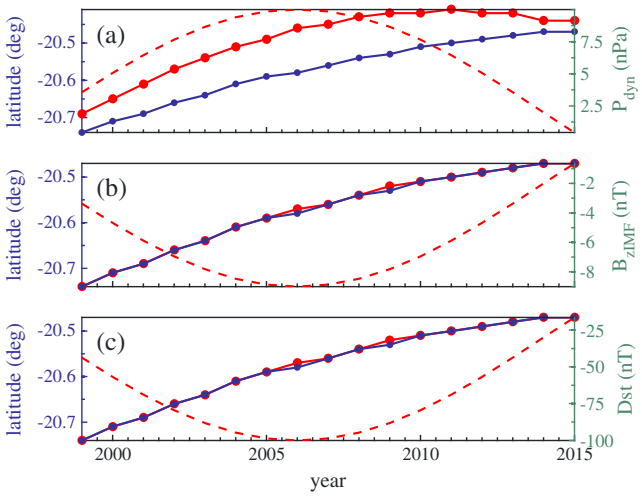

Figure 11. Variations of the latitudinal point of the minimum geomagnetic field (B_{min}) with respect to external factors. The blue solid curves represent the results for the case with P_{dyn} = 0.5 nPa, B_{yIMF} = 0 nT, B_{zIMF} = 0 nT, and *Dst* = 0 nT. From top to bottom, (a) change P_{dyn} only, (b) change B_{zIMF} only, and (c) change *Dst* only, as shown by the red dashed curves. The corresponding variations of the latitudinal point of B_{min} are indicated by the red solid curves.

the 11 years (1999–2009) of the NOAA 15 proton flux measurements. The inverse correlation between the area and strength of the SAA proton flux and the $F_{10.7}$ flux, as illustrated in Figures 3, 5, and 9 confirms previously published results [*Huston et al.*, 1998; *Dachev et al.*, 1999; *Li et al.*, 2001; *Fürst et al.*, 2009; *Kuznetsov et al.*, 2010; *Casadio and Arino*, 2011]. There can be two major reasons responsible for this solar cycle effect. One is the solar cycle variation of Cosmic Ray Albedo Neutron Decay (CRAND) process, which is believed to be a main source of the protons in the inner radiation belt [*Singer*, 1958]. During the solar minimum, with more cosmic rays interacting with the atmospheric nuclei, the Cosmic Ray Albedo Neutron Decay (CRAND) process is enhanced, thus causing enhancements of the proton flux. The other reason can be the solar cycle variation of the atmospheric loss process [*Farley and Walt*, 1971; *Miyoshi et al.*, 2000]. Earth's upper atmosphere can get heated by the solar extreme ultraviolet (EUV) radiation and then extends to higher altitudes. As a consequence, an increase in the output of EUV during the solar maximum leads to a higher neutral density in the SAA and a higher absorption of the trapped protons as well. Thus, the two above processes both can increase the low altitude proton fluxes during the solar minimum. *Miyoshi et al.* [2000] only considered the effect of the latter by assuming that the neutron flux was time independent. They found that the observed and simulated results agree well only at $L < 1.16$. Corresponding to a height of 808 km in the SAA, *L* value ranges from 1.1 to 1.3, and the solar cycle variation can be primarily controlled by the above two factors. There tends to be little difference in the amplitude of the variation for the four considered MEPED proton energy channels. Further investigations are required to analyze to which extent the CRAND process and the atmospheric loss process depend on the proton energy at low altitudes. In addition, our results show that the maximum proton flux tends to increase in a total solar cycle, which is consistent with the secular change of the geomagnetic field. The decrease of the geomagnetic field at a fixed altitude within a solar cycle can lower the inner boundary of the inner zone [*Jiao et al.*, 1999]. Accordingly, the proton flux at the height of 808 km can increase along with the inward movement of the inner radiation belt.

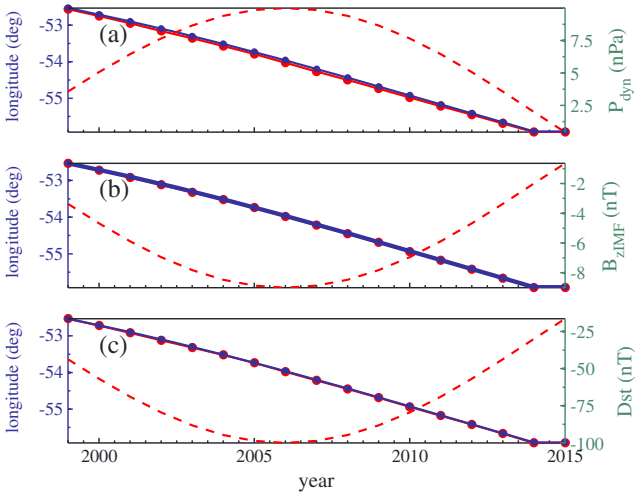

Figure 12. Same as in Figure 11, except for variations of the longitudinal point of B_{min}.

The protons with energies above 70 MeV at 808 km have a phase lag of 685 days in the anticorrelation relationship with solar activity during the 23rd solar cycle, as indicated in Figure 5. Similar hysteresis effect was also obtained in different coordinates by previous studies [*Huston et al.*, 1996, 1998; *Huston and Pfitzer*, 1998; *Kuznetsov et al.*, 2010]. Since the time

required for the neutral atmospheric density to get heated and reach the height of 808 km is only a few minutes, much shorter than the timescale of the phase lag, the value of the phase lag is dominantly determined by the proton lifetime. The lifetime of protons against energy loss with $E > 30$ MeV can be greater than 30 years [*Pu et al.*, 2005]. At typical LEO altitudes, the proton lifetimes, which is mainly attributed to the atmospheric loss [*Filz and Holeman*, 1965; *Heynderickx et al.*, 1996], are of the order of a few years. In addition, the proton lifetime due to Coulomb scattering in the atmosphere is energy and altitude dependent [*Wentworth et al.*, 1959]. According to the barometric law,

$$\rho \propto \exp(-mgh/kT) \tag{3}$$

the density of atmospheric constituents decreases with altitude. Consequently, the lifetime of protons increases with L shell. According to our analysis results, the protons > 70 MeV at the height of 808 km, with a latitude of −25° and a longitude of −50°, are located at $L \sim 1.3$. Their lifetime is estimated to be of the order of a few years during the solar maximum [*Miyoshi et al.*, 2000], consistent with the delay time of 685 days obtained in this study. In addition, the phase lag varies with solar cycle. In the even 22nd cycle the phase lag is lower than that in the odd 21st and 23rd SA cycles [*Kuznetsov et al.*, 2010].

As shown in Figure 9, the SAA area decreases at a speed about 0.59 deg^2 per day during the solar maximum and increase at a speed about 0.47 deg^2 per day during the solar minimum, which can be largely attributed to the variation of the neutral atmosphere density that has been found to increase rapidly during the solar maximum and decrease slowly during the solar minimum [*Miyoshi et al.*, 2000]. In addition, the area is expanded in a total solar cycle, which may be caused by the decrease of the geomagnetic field strength and the resultant inward extension of the inner radiation belt [*Jiao et al.*, 1999].

Figure 7 tells that the center of the SAA longitudinal drifts faster during the solar minimum than the solar maximum. While a number of studies reported the westward drift of the SAA longitudinal position of the proton flux peak [*Konradi et al.*, 1994; *Bühler et al.*, 1996; *Badhwar*, 1997; *Grigoryan et al.*, 2005, 2008], there was very little investigation on the drift velocity characteristics over a time span of an entire solar cycle until this study. *Fürst et al.* [2009] pointed out that it might be associated with geomagnetic jerks. Our present investigation clearly demonstrates a good correlation between the westward drift rate and the $F_{10.7}$ flux, strongly suggesting a robust connection between these two quantities in terms of the strength of the solar activity.

Apart from the northward drift [*Badhwar*, 1997; *Grigoryan et al.*, 2008], the SAA latitudinal position of the proton flux peak is also found to drift southward during the solar maximum. The northward drift is consistent with the secular variation of the geomagnetic field, which also drifts northward gradually. The southward drift trend during the solar maximum is a new finding, which however requires further studies to understand its mechanism.

From Figure 10 we note that the internal magnetic field drifts westward and northward gradually and slowly. Neither the longitudinal nor latitudinal positions of the geomagnetic field minimum show clear solar cycle variations. Upon the assumption that the drift of the SAA proton flux maximum is directly related to the variation of the local magnetic field minimum, it may be reasonable to speculate that the results obtained in Figures 7 and 8 can be more likely to be caused by external factors associated with the solar activity. This proposed connection between the drift and the solar activity has been checked with the results shown in Figures 11 and 12. It is clear that the latitudinal position of the geomagnetic field minimum (red solid line) drifts southward quickly after the solar wind dynamic pressure increases to a high value. This behavior is distinct from that with constant, low solar wind dynamic pressure ($P_{dyn} = 0.5$ nPa, blue solid line), suggesting that increase in P_{dyn} favor the southward latitudinal drift of the SAA. In a statistical sense, the solar wind dynamic pressure is significantly higher during the solar maximum than the solar minimum and thus results in enhanced compression of the Earth's magnetic field during the solar maximum. As a consequence, the location of the minimum magnetic field can go southward. In contrast, Figures 11b and 11c show that the other two indices, B_{zIMF} and *Dst*, have little effect on the variation of the position of the geomagnetic field minimum in a solar cycle. In addition, the temporal evolution of the longitudinal position of the SAA B_{min} shows no clear dependence on any of the three considered indices (Figure 12). We note that this does not demonstrate that the longitude of local particle maximum is insensitive to the solar activity, since these results are obtained upon the assumption that the local particle maximum is closely correlated with the

local magnetic field minimum. It is also possible that the solar activity can influence the distribution of the SAA proton flux directly, which needs more data from different satellite sources to testify.

5. Conclusive Remarks

To analyze the long-term variation of the inner zone proton flux in the South Atlantic Anomaly (SAA), we have adopted the proton flux data measured by NOAA 6, NOAA 10, NOAA 12, and NOAA 15 from 1980 through 2009 and performed reasonable Gaussian fits for a statistical analysis. Our main conclusions are summarized as follows:

1. There is an anticorrelation and a phase lag between the measurements of SAA proton fluxes and $F_{10.7}$ fluxes. The local maximum of the proton flux tends to increase over an entire solar cycle. The variation trends are approximately the same with respect to the four energy channels in our research. The phase lag in the anticorrelation relationship differs in different solar cycles.
2. The longitudinal center of the SAA drifts faster during the solar minimum than the solar maximum. This trend is different from the secular variation of the geomagnetic field. The westward drift rate shows a good correlation with the $F_{10.7}$ flux, which however requires further investigations.
3. The maximal latitudinal position of the SAA proton flux has different direction drifts within a solar cycle. Such an opposite trend of long-term drift profile may be associated with the solar wind dynamic pressure.
4. The area of the SAA and the $F_{10.7}$ flux is anticorrelated. The SAA area expands within an entire solar cycle. It also shows a rapid decrease during the solar maximum and a slow increase during the solar minimum.

Acknowledgments

We thank the NOAA Space Weather Prediction Center for providing the POES data (http://www.ngdc.noaa.gov/stp/satellite/poes/dataaccess.html) and the National Geophysical Data Center for providing the $F_{10.7}$ indices (http://www.swpc.noaa.gov/ftpmenu/indices/old_indices.html). This study is supported by the National Natural Science Foundation of China (NSFC) under the grants 41204119, 41204120, 41274177, 41374167, and 41104113. B.N. also acknowledges the support from the Fundamental Research Funds for the Central Universities under the grant 2042014kf0251.

Yuming Wang thanks the reviewers for their assistance in evaluating this paper.

References

Badhwar, G. D. (1997), Drift rate of the South Atlantic Anomaly, *J. Geophys. Res.*, *102*(A2), 2343–2349.

Badhwar, G. D., A. Konradi, L. A. Braby, W. Atwell, and F. A. Cucinotta (1994), Measurements of trapped protons and cosmic rays from recent shuttle flights, *Adv. Space Res.*, *14*(10), 67–72.

Bühler, P., L. Desorgher, A. Zehnder, E. Daly, and L. Adams (1996), Observations of the low Earth orbit radiation environment from MIR, *Radiat. Meas.*, *26*(6), 917–921.

Casadio, S., and O. Arino (2011), Monitoring the South Atlantic Anomaly using ATSR instrument series, *Adv. Space Res.*, *48*(6), 1056–1066.

Dachev, T. P., B. Tomov, Y. N. Matviichuk, R. Koleva, J. Semkova, V. Petrov, V. Benghin, Y. V. Ivanov, V. Shurshakov, and J. Lemaire (1999), Solar cycle variations of MIR radiation environment as observed by the LIULIN dosimeter, *Radiat. Meas.*, *30*(3), 269–274.

Dragt, A. J. (1971), Solar cycle modulation of the radiation belt proton flux, *J. Geophys. Res.*, *76*(10), 2313–2344.

Evans, D. S., and M. S. Greer (2000), *Polar Orbiting Environmental Satellite Space Environment Monitor-2: Instrument Description and Archive Data*, U.S. Dep. of Commer., Natl. Oceanic and Atmos. Admin., Oceanic and Atmos. Res. Lab., Space Environ. Cent., Boulder, Colo.

Farley, T. A., and M. Walt (1971), Source and loss processes of protons of the inner radiation belt, *J. Geophys. Res.*, *76*(34), 8223–8240.

Fürst, F., J. Wilms, R. E. Rothschild, K. Pottschmidt, D. M. Smith, and R. Lingenfelter (2009), Temporal variations of strength and location of the South Atlantic Anomaly as measured by RXTE, *Earth Planet. Sci. Lett.*, *281*(3-4), 125–133.

Filz, R. C., and E. Holeman (1965), Time and altitude dependence of 55-MeV trapped protons, August 1961 to June 1964, *J. Geophys. Res.*, *70*(23), 5807–5822.

Ginet, G. P., D. Madden, B. K. Dichter, and D. H. Brautigam (2007), Energetic proton maps for the South Atlantic Anomaly, in *IEEE Radiation Effects Data Workshop*, pp. 1–8, IEEE, Honolulu, Hawaii.

Grigoryan, O., A. Petrov, V. Romashova, and V. Bengin (2005), On the drift of the South Atlantic Anomaly, *WDS'05 Proc. Contributed Papers, Part II*, *5*, 251–256.

Grigoryan, O. R., V. V. Romashova, and A. N. Petrov (2008), SAA drift: Experimental results, *Adv. Space Res.*, *41*(1), 76–80.

Hell, N. (2010), *The Evolution of the South Atlantic Anomaly Measured by RHESSI*, Bachelorarbeit, Friedrich-Alexander-Universität Erlangen-Nürnberg, Germany.

Heynderickx, D. (1996), Comparison between methods to compensate for the secular motion of the South Atlantic Anomaly, *Radiat. Meas.*, *26*(3), 369–373.

Heynderickx, D., J. Lemaire, and E. Daly (1996), Historical review of the different procedures used to compute the L-parameter, *Radiat. Meas.*, *26*(3), 325–331.

Huston, S., and K. Pfitzer (1998), Space environment effects: Low-altitude trapped radiation model, *Tech. Rep. NASA/CR-1998-208593, Contract NAS8-40295*, Marshall Space Flight Center, NASA, Huntsville, Ala.

Huston, S., G. Kuck, and K. Pfitzer (1996), Low-altitude trapped radiation model using TIROS/NOAA data, in *Radiation Belts: Models and Standards*, vol. 97, edited by J. F. Lemaire pp. 119–122, AGU, Washington, D. C.

Huston, S., G. Kuck, and K. Pfitzer (1998), Solar cycle variation of the low-altitude trapped proton flux, *Adv. Space Res.*, *21*(12), 1625–1634.

Jiao, W.-X., Z.-Y. Pu, X.-H. Fang, and S. Fu (1999), The radiation environment within the South Atlantic Anomaly region and the calculating trapped particles fluxes for low orbital satellite, *Chin. J. Geophys. Chin. Ed.*, *42*(2), 163–168.

Konradi, A., G. Badhwar, and L. Braby (1994), Recent space shuttle observations of the South Atlantic Anomaly and the radiation belt models, *Adv. Space Res.*, *14*(10), 911–921.

Kurnosova, L., T. Kolobyanina, V. Logachev, L. Razorenov, I. Sirotkin, and M. Fradkin (1962), Discovery of radiation anomalies above the South Atlantic at heights of 310–340 km, *Planet. Space Sci.*, *9*(8), 513–516.

Kuznetsov, N. V., N. I. Nikolaeva, and M. I. Panasyuk (2010), Variation of the trapped proton flux in the inner radiation belt of the Earth as a function of solar activity, *Cosmic Res.*, *48*(1), 80–85.

Li, X., D. N. Baker, S. G. Kanekal, M. Looper, and M. Temerin (2001), Long term measurements of radiation belts by SAMPEX and their variations, *Geophys. Res. Lett.*, *28*(20), 3827–3830.

McIlwain, C. E. (1966), Magnetic coordinates, *Space Sci. Rev.*, *5*(5), 585–598.

Miyoshi, Y., A. Morioka, and H. Misawa (2000), Long term modulation of low altitude proton radiation belt by the Earth's atmosphere, *Geophys. Res. Lett.*, *27*(14), 2169–2172.

Nakano, G., and H. Heckman (1968), Evidence for solar-cycle changes in the inner-belt protons, *Phys. Rev. Lett.*, *20*(15), 806–809.

Olsen, N., and M. Mandea (2007), Investigation of a secular variation impulse using satellite data: The 2003 geomagnetic jerk, *Earth Planet. Sci. Lett.*, *255*(1–2), 94–105.

Pu, Z. Y., L. Xie, W. X. Jiao, S. Y. Fu, X. H. Fang, Q. G. Zong, and D. Heynderickx (2005), Drift shell tracing and secular variation of inner zone high energy proton environment in the SAA, *Adv. Space Res.*, *36*(10), 1973–1978.

Shea, M., and D. Smart (1990), A summary of major solar proton events, *Sol. Phys.*, *127*(2), 297–320.

Singer, S. F. (1958), Trapped albedo theory of the radiation belt, *Phys. Rev. Lett.*, *1*, 181–183.

Tsyganenko, N. A. (1995), Modeling the Earth's magnetospheric magnetic field confined within a realistic magnetopause, *J. Geophys. Res.*, *100*(A4), 5599–5612.

Wentworth, R. C., W. MacDonald, and S. Singer (1959), Lifetimes of trapped radiation belt particles determined by Coulomb scattering, *Phys. Fluids*, *2*, 499–599.

Xie, L., Z. Pu, W. Jiao, and S. Fu (2005), The secular variation of inner zone high energy proton environment in the SAA, *Sci. Chin. Ser. D*, *48*(12), 2123–2130.